

Gamma-ray performance study of the HERD payload

**L. Fariña^{a,*}, L. Jouvin^a, J. Rico^a, N. Mori^b, F. Gargano^c, V. Formato^d, F. de Palma^e,
C. Pizzolotto^f, J. Casaus^g, M. N. Mazziota^c, X. Wu^h, P. Bordasⁱ, D. Gascónⁱ,
D. Sukhonos^h, A. Tykhonov^h, C. Altomare^c, L. Silveri^j, and D. Gasparri^d on behalf
of the HERD Collaboration**

(a complete list of authors can be found at the end of the proceedings)

^a*Institut de Física d'Altes Energies (IFAE), The Barcelona Institute of Science and Technology (BIST),
E-08193 Bellaterra, Barcelona, Spain*

^b*Istituto Nazionale di Fisica Nucleare, Sezione di Firenze,
Firenze, Italy*

^c*Istituto Nazionale di Fisica Nucleare, Sezione di Bari,
Bari, Italy*

^d*Istituto Nazionale di Fisica Nucleare, Sezione di Roma Tor Vergata,
Rome, Italy*

^e*Università del Salento and Istituto Nazionale di Fisica Nucleare, Sezione di Lecce,
Lecce, Italy*

^f*Istituto Nazionale di Fisica Nucleare, Sezione di Trieste,
Trieste, Italy*

^g*Centro de Investigaciones Energéticas, Medioambientales y Tecnológicas (CIEMAT),
E-28040 Madrid, Spain*

^h*Département de Physique Nucléaire et Corpusculaire (DPNC), Université de Genève,
Genève, Switzerland*

ⁱ*Dept. Física Quàntica i Astrofísica, Institut de Ciències del Cosmos (ICCUB), Universitat de Barcelona
(IEEC-UB),
Barcelona, Spain*

^j*Gran Sasso Science Institute, L'Aquila, Italy and INFN Laboratori Nazionali del Gran Sasso,
Assergi, L'Aquila, Italy*

E-mail: lfarina@ifae.es

*Presenter

The High Energy cosmic-Radiation Detection (HERD) facility has been proposed as a space astronomy payload onboard the future China's Space Station. HERD is planned for operation starting around 2027 for about 10 years. In addition to the unprecedented sensitivity for dark matter searches and cosmic-ray measurements up to the knee energy, it should perform gamma-ray monitoring and full sky survey from few hundred MeV up to tens of TeV. We present the first study of the HERD gamma-ray performance obtained with full simulations of the whole detector geometry. HERD will be a cubic detector composed with 5 active faces. We present a study conducted inside the HERD analysis software package, which includes a detailed description of the detector materials. In this work we present the HERD effective area, the point spread function and the resulting gamma-ray sensitivity.

1. Introduction

Space-based gamma-ray experiments are prone to the constraints that traditionally plague satellite platforms, namely their tight mass and volume budgets. However, they remain interesting because of their large duty cycle (limited mostly by detector deadtime and passage over the South Atlantic Anomaly) and their longevity (they do not have large requirements for consumables).

The *Fermi* satellite, launched in 2008 and currently still in operation, is arguably the most successful mission to date. Its LAT instrument has been responsible for the detection and identification of well over 5000 point sources, and it has been involved in several other major discoveries like the extended Fermi bubbles [1]. However, as it approaches the end of its operational life, a solution will be needed to ensure the continuity of observations from space. This is of particular relevance considering that the most advanced generation of ground-based gamma-ray observatories (CTA, LHAASO), is scheduled to come online in the following years.

With its scheduled launch date, the HERD mission is well poised to be able to take over in this role. Additionally, some key differences in its design will allow for a new look into the gamma-ray sky.

2. HERD geometry and subdetectors

HERD is a future multimessenger astroparticle detector, to be installed aboard the Chinese Space Station circa 2027. The HERD collaboration currently comprises more than 200 members across more than 50 different Chinese, Italian, Swiss and Spanish institutes.

HERD features an innovative design, to enable simultaneous operation as a cosmic and gamma ray experiment [2]. Both the top and the lateral sides of the detector are instrumented, in order to maximize utilization of its available field of view.

From the outside in, particles first cross the Silicon Charge Detector (SCD), composed of silicon microstrip detectors, which is used to reconstruct the charge of incoming cosmic rays. Next up is the Plastic Scintillator Detector (PSD), composed of two layers of staggered scintillator tiles and which serves as the veto system for gamma-rays.

The Fliber Tracker (FIT) is the main instrument used for reconstructing the the gamma-ray incident direction. It consists of seven double layers, with each double layer consisting of mats of scintillating fibers that span the whole length of each face along alternating directions. Within each mat, fibers are placed with a pitch of $\sim 250 \mu\text{m}$. The current HERD configuration does not include tungsten foils within the tracker as in comparable gamma-ray detectors. This significantly reduces γ conversion efficiency in comparison with other gamma-ray detectors that do include them. In exchange for this, the scattering of charged particles within the tracker is greatly reduced, which allows for very precise track reconstruction, down to 0.1 deg for γ s above 10 GeV.

At the center of HERD is a CALORimeter (CALO), made of LYSO crystals and consisting of more than 7500 individually read out cubic segments. Its optical depth will allow for fine energy reconstruction, down to 1 % for γ s above 200 GeV [2].

Finally, the Transition Radiation Detector (TRD) is there to calibrate the CALO response to TeV protons.

3. Simulations and analysis

The Monte Carlo productions in this work are generated and analyzed using the official Herd-Software tools.

First, the interactions between the particles and the detector volumes are simulated using GGS (Generic Géant4 Simulation), a program based on Géant4 [3]. Primary photons are generated with different initial energy and for different incidence angles with regard to the faces of the detector. We run two studies, one for the top face of HERD and one for the lateral face oriented towards the port side, which we use as a benchmark for the other three lateral faces. The samples in this work total $4 \cdot 10^7$ gamma rays with energies in the range of 0.01–100 GeV.

Once the particle interactions and energy depositions in the detector model are mapped, they are digitized into the actual signals that will be reported by HERD. This step and the subsequent analysis of these signals are handled within the EventAnalysis framework.

4. Effective Area

The current design for the low energy γ trigger system features a threshold for energy deposition in the CALO that is quite high and so severely restricts the performance of HERD in the lowest energy ranges. Studies are underway for an alternative trigger system free of this constraint (e.g based only on signals from FIT and PSD). On the other hand gamma-rays above ~ 15 GeV are always triggered by the High Energy Trigger system. In this study we consider a proxy trigger designed to mimic the capabilities of an eventual extended Low Energy Gamma trigger (currently under study).

The events selected are chosen such that they verify the following cuts:

- The tracks of the primary gamma-rays intersect the FIT plane under study for each generation
- Pair conversion takes place within the volume occupied by the FIT.
- After conversion, both the e^+ and the e^- leave enough hits in the FIT sensitive elements to produce a good reconstruction of the primary track. Specifically, we request that there are ≥ 3 hits for each particle in each of the X/Y layers. In practice, this rejects any conversions that take place in the last two double layers of the FIT
- Finally, we ask that the total energy deposition in the CALO be at least 50% of the primary energy ends up deposited in the CALO. This removes events with tracks that miss or merely graze the CALO and ensures that the true energy of the particles could eventually be reconstructed to a certain accuracy.

We study the effective area as a function of the energy of the primary and the incidence angle (taken between the normal of the face and the primary's track). The effective area is calculated as the product of the generation area perpendicular to the generation direction and the detection efficiency, where the detection efficiency can be estimated by the ratio of triggered to generated particles:

$$A_{eff}(E, \theta) = \frac{N_{trigger}(E, \theta)}{N_{gen}(E, \theta)} A_{gen}(E, \theta) \quad (1)$$

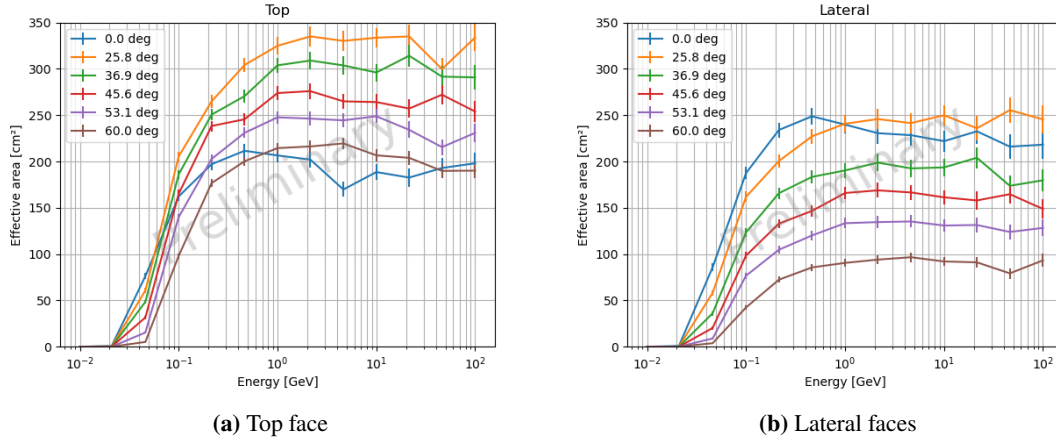


Figure 1: Effective area as a function of the incidence angle and primary energy

The resulting effective area (Fig. 1) is a factor ~ 50 smaller than that of *Fermi*-LAT, a difference mostly due to the absence of tungsten conversion layers within the FIT. Considering also the improved field of view in HERD, the ratio of acceptances is reduced to ~ 10 – 20 times.

5. PSF

The algorithm for track reconstruction to be used by HERD is currently being developed. In the meantime, we again resort to using a simplistic proxy to estimate the performance of HERD in this regard. The process is as follows:

- Look for pairs of hits in consecutive X/Y pairs of layers. Pairs of hits in consecutive layers are needed, since each layer only carries information on the coordinates that are perpendicular to the length of the fiber
- Smear the positions of the hits to the precision defined by the FIT, i.e. $250\ \mu\text{m}$.
- From these pairs of hits, reconstruct the position of a combined hit:
 - For the coordinate normal to the detector plane, take the average of the coordinates in both layers
 - For the coordinates along the detector plane, take the coordinate of the layer sensitive in that direction
- Fit two tracks to these points, one for the e^+ and one for the e^-
- Take the average direction of both tracks as the direction of the reconstructed γ track
- Calculate the angle between the reconstructed and the true tracks
- Finally, report the 68% containment radius in every energy bin

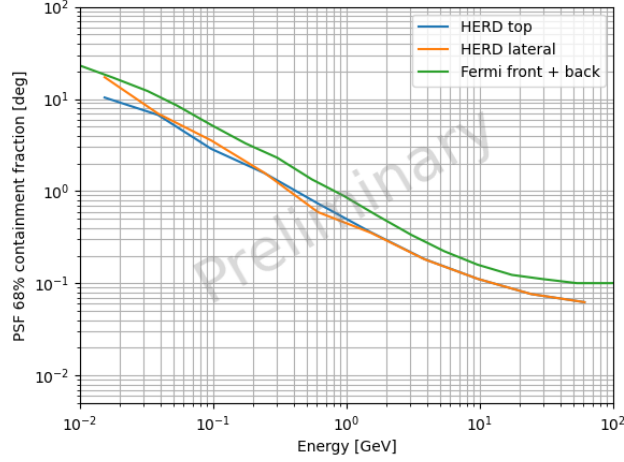


Figure 2: PSF for the top and lateral faces computed with the method described. The *Fermi*-LAT average PSF is included for reference.

At energies higher than ~ 10 GeV the resolution limits of the FIT cause the PSF to saturate at values below 0.1 deg (see Fig. 2), but below this value it may be possible to improve on the resolution presented in this work by using better reconstruction methods. Even so, the performance of the FIT, together with the absence of W foils between the tracking layers, make the HERD PSF already quite competitive.

6. Point-like source differential sensitivity

From these quantities we can produce a first approximation for the point-like source differential sensitivity of the detector, i.e. the necessary source flux to produce a 5σ detection in each energy bin. We consider here 4 bins per decade in energy, and a minimum requirement of 10 photons to report a detection.

To this end, we have repurposed the *fermitools* to allow us to load the effective area tables depicted above, and we use the *Fermi*-LAT PSF3 as it is most similar to the HERD PSF we are reporting here.

For the source model, we assume a point-like source with an index 2 power law spectrum. For the background we use the *Fermi*-LAT isotropic background model for P8R3_SOURCE events, as a substitute for an isotropic background model that takes into account the background produced by cosmic ray interactions with the outer subdetectors of HERD and/or components of the CSS. We also use the *Fermi*-LAT galactic emission model `gll_iem_v07.fits`, to produce sensitivity curves for targets near the galactic plane.

The resulting curves can be seen in Fig. 3. For pointings away from the galactic plane, the best sensitivity of $\sim 10^{-6}$ MeVcm $^{-2}$ s $^{-1}$ is achieved at energies ~ 1 GeV, while for pointings towards the galactic plane the sensitivity is an order of magnitude worse, at $\sim 10^{-5}$ MeVcm $^{-2}$ s $^{-1}$ for ~ 10 GeV gamma-rays

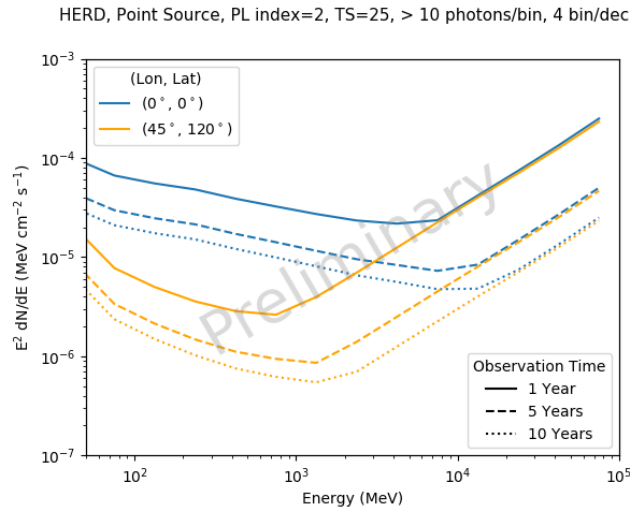


Figure 3: HERD differential sensitivity to point-like sources for sample galactic and extragalactic pointings at 1, 5 and 10 yr

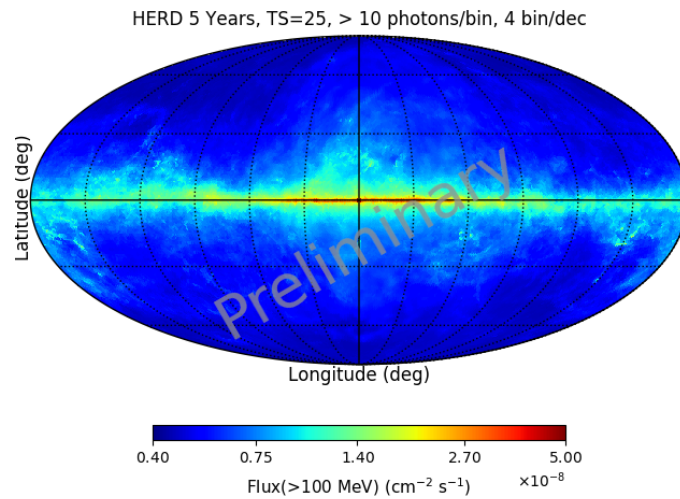


Figure 4: HERD 5-year skymap for gamma-rays above 100 MeV

This procedure also allows for generating estimates of the sky map, like the one depicted in Fig. 4 for 5 years of observations.

7. Conclusion

In this work we have reported on the baseline capabilities for HERD in the detection of low energy gamma-rays (in the range 0.01–100 GeV). This work can and will be updated e.g. as the designs of the low energy gamma-ray trigger system or the track reconstruction procedure are updated, or in case of any changes are made to the fiducial HERD design. Nevertheless, with the present study we can already say that the superior field of view of the detector and its energy and angular resolution will lead to adequate performance in the detection of gamma-rays. With the

performance we describe here, HERD will become a reference space instrument for gamma-ray observations in the near future.

Acknowledgements

This work has received funding from the Spanish Ministerio de Ciencia, Innovación y Universidades and the Agencia Estatal de Investigación through the program Subprograma Estatal de Generación del Conocimiento (ESP2017-89979-P) and from the FSE under the program Ayudas predoctorales of the Ministerio de Ciencia, Innovación y Universidades (PRE2019-091232)

References

- [1] Fermi-LAT Collaboration et al. Fermi large area telescope fourth source catalog. *Astrophysical Journal Supplement*, 247:33, 2020.
- [2] Yongwei Dong, Shuangnan Zhang, and Giovanni Ambrosi. Overall Status of the High Energy Cosmic Radiation Detection Facility Onboard the Future China's Space Station. *PoS, ICRC2019:062*, 2019. doi: 10.22323/1.358.0062.
- [3] Nicola Mori. Ggs: A generic geant4 simulation package for small- and medium-sized particle detection experiments. *Nuclear Instruments and Methods in Physics Research Section A: Accelerators, Spectrometers, Detectors and Associated Equipment*, 1002:165298, Jun 2021. ISSN 0168-9002. doi: 10.1016/j.nima.2021.165298. URL <http://dx.doi.org/10.1016/j.nima.2021.165298>.

Full Authors List: HERD Collaboration

O. Adriani²⁶, F. Alemanno²⁷, R. Aloisio²⁷, C. Altomare²³, G. Ambrosi³⁴, Q. An¹⁰, M. Antonelli⁴⁵, P. Azzarello³⁷, L. Bai⁸, Y.L. Bai³, T.W. Bao¹, M. Barbanera³⁴, F.C.T. Barbato²⁷, P. Bernardini³⁰, E. Berti²⁶, B. Bertucci³⁵, X.J. Bi¹, G. Bigongiari³⁶, M. Bongio²⁶, V. Bonvicini⁴⁵, P. Bordas⁴⁰, V. Bosch-Ramon⁴⁰, S. Bottai²⁵, P. Brogi³⁶, F. Cadoux³⁷, D. Campana³¹, W.W. Cao³, Z. Cao¹, J. Casaus³⁹, E. Catanzani³⁵, P. W. Cattaneo³³, J. Chang^{9,13}, Y.H. Chang²¹, G.M. Chen¹, Y. Chen¹⁵, F. Cianetti³⁵, A. Comerma^{40,41}, D. Cortis²⁸, X.H. Cui¹³, X.Z. Cui¹, C. Dai⁵, Z.G. Dai¹⁵, R. D'Alessandro²⁶, S. De Gaetano²⁴, I. De Mitri²⁷, F. de Palma³⁰, V. Di Felice⁵⁰, A. Di Giovanni²⁷, M. Di Santo²⁷, L. Di Venere²⁴, J.N. Dong^{6,7}, Y.W. Dong¹, G. Donvito²³, M. Duranti³⁴, D. D'Urso⁴⁹, C. Evoli²⁷, K. Fang¹, L. Fariña⁴², Y. Favre³⁷, C.Q. Feng¹⁰, H. Feng¹⁶, H.B. Feng⁵, Z.K. Feng⁵, N. Finetti²², V. Formato⁵⁰, J. M. Frieden⁴⁴, P. Fusco²⁴, J.R. Gao³, F. Gargano²³, D. Gascon-Fora⁴⁰, D. Gasparrini⁵⁰, N. Giglietto²⁴, F. Giovacchini³⁹, S. Gomez⁴⁰, K. Gong¹, Q.B. Gou¹, R. Guida⁴⁶, D.Y. Guo¹, J.H. Guo⁹, Y.Q. Guo¹, H.H. He¹, H.B. Hu¹, J.Y. Hu^{1,2}, P. Hu^{1,2}, Y.M. Hu⁹, G.S. Huang¹⁰, J. Huang¹, W.H. Huang^{6,7}, X.T. Huang^{6,7}, Y.B. Huang⁵, Y.F. Huang¹⁵, M. Ionica³⁴, L. Jouvin⁴², A. Kotenko³⁷, D. Kyratzis²⁷, D. La Marra³⁷, M.J. Li^{6,7}, Q.Y. Li^{6,7}, R. Li³, S.L. Li^{1,2}, T. Li^{6,7}, X. Li⁹, Z. Li¹⁷, Z.H. Li^{1,2}, E.W. Liang⁵, M.J. Liang^{1,2}, C.L. Liao⁸, F. Licciulli²³, S.J. Lin¹, D. Liu^{6,7}, H.B. Liu⁵, H. Liu⁸, J.B. Liu¹⁰, S.B. Liu¹⁰, X. Liu^{1,2}, X.W. Liu⁵, Y.Q. Liu¹, F. Loparco²⁴, S. Loporchio²³, X. Lu⁵, J.G. Lyu⁴, L.W. Lyu³, P. Maestro³⁶, E. Mancini³⁴, R. Manera⁴⁰, J. Marin³⁹, P. S. Marrocchesi³⁶, G. Marsella⁵³, G. Martinez³⁹, M. Martinez⁴², D. Marzullo⁴⁷, J. Mauricio⁴⁰, E. Mocchiutti⁴⁵, G. Morettini³⁵, N. Mori²⁵, L. Mussolin³⁵, M. Nicola Mazziotta²³, A. Oliva⁵¹, D. Orlandi²⁸, G. Osteria³¹, L. Pacini²⁵, B. Panico³¹, F.R. Pantaleo²⁴, S. Papa⁴⁶, P. Papini²⁵, J.M. Paredes⁴⁰, A. Parenti²⁷, M. Pauluzzi³⁵, M. Pearce⁴³, W.X. Peng¹, F. Perfetto³¹, C. Perrina⁴⁴, G. Perrotta⁴⁶, R. Pillera²⁴, C. Pizzolotto⁴⁵, R. Qiao¹, J.J. Qin³, L. Quadran^{51,52}, Z. Quan¹, A. Rappoldi³³, G. Raselli³³, X.X. Ren^{6,7}, F. Renno⁴⁶, M. Ribo⁴⁰, J. Rico⁴², M. Rossella³³, F. Ryde⁴³, A. Sanmukh⁴⁰, V. Scotti³², D. Serini²³, D.L. Shi³, Q.Q. Shi^{6,7}, L. Silveri²⁷, O. Starodubtsev²⁵, D.T. Su¹², M. Su²⁰, D. Sukhono³⁷, A. Suma⁴⁶, X.L. Sun¹, Z.T. Sun^{1,2}, A. Surdo²⁹, Z.C. Tang¹, A. Tiberio²⁶, A. Tykhonov³⁷, V. Vagelli⁴⁸, E. Vannuccini²⁵, M. Velasco³⁹, R. Walter³⁸, A.Q. Wang^{6,7}, B. Wang³, J.C. Wang¹⁴, J.M. Wang¹, J.J. Wang^{1,2}, L. Wang¹³, M. Wang^{6,7}, R.J. Wang¹, S. Wang⁹, X.Y. Wang¹⁵, X.L. Wang¹⁰, Z.G. Wang¹, D.M. Wei⁹, J.J. Wei⁹, B.B. Wu¹, J. Wu¹⁹, L.B. Wu²⁷, X. Wu³⁷, X.F. Wu⁹, Y.L. Xin⁸, M. Xu¹, Z.Z. Xu¹⁰, H.R. Yan¹⁷, Y. Yang³, P.F. Yin¹, Y.W. Yu¹⁸, Q. Yuan⁹, G. Zampa⁴⁵, N. Zampa⁴⁵, M. Zha¹, C. Zhang¹, F.Z. Zhang^{1,2}, L. Zhang¹, L. Zhang¹¹, L.F. Zhang^{1,2}, S.N. Zhang^{1,2}, Y. Zhang⁹, Y.L. Zhang¹⁰, Z.G. Zhao¹⁰, J.K. Zheng³, Y.L. Zhou⁵, F.R. Zhu⁸, K.J. Zhu⁴

¹ Key Laboratory of Particle and Astrophysics, Chinese Academy of Sciences, Beijing, China

² University of Chinese Academy of Sciences, Beijing, China

³ Xi'an Institute of Optics and Precision Mechanics of CAS, Xi'an, China

⁴ Institute of High Energy Physics, Chinese Academy of Sciences, Beijing, China

⁵ School of Physical Science and Technology, Guangxi University, Nanning, China

⁶ Institute of Frontier and Interdisciplinary Science, Shandong University, Qingdao, China

⁷ Key Laboratory of Particle Physics and Particle Irradiation, Ministry of Education, China

⁸ School of Physical Science and Technology, Southwest Jiaotong University, Chengdu, China

⁹ Key Laboratory of Dark Matter and Space Astronomy, Purple Mountain Observatory, Chinese Academy of Sciences, Nanjing 210023, China

¹⁰ Department of Modern Physics, University of Science and Technology of China, Hefei, China

¹¹ Department of Astronomy, Yunnan University, Kunming, China

¹² North Night Vision Technology co. Ltd., Kunming, China

¹³ National Astronomical Observatories, Chinese Academy of Sciences, Beijing 100101, China

¹⁴ Yunnan Astronomical Observatory, Chinese Academy of Sciences, Kunming, China

¹⁵ School of Astronomy and Space Science, Nanjing University, Nanjing, China

¹⁶ Department of Astronomy, Tsinghua University, Beijing, China

¹⁷ Department of Astronomy, Peking University, Beijing, China

¹⁸ Institute of Astrophysics, Central China Normal University, Wuhan, China

¹⁹ Department of Physics, China University of Geosciences, Wuhan, China

²⁰ The University of Hong Kong, Hong Kong, China

²¹ Institute of Physics, Academia Sinica, Taipei, Taiwan

²² Università dell'Aquila and Istituto Nazionale di Fisica Nucleare, Sezione di Firenze, Firenze, Italy

²³ Istituto Nazionale di Fisica Nucleare, Sezione di Bari, Bari, Italy

²⁴ Dipartimento di Fisica "M.Merlin" dell'Università e del Politecnico di Bari, and Istituto Nazionale di Fisica Nucleare, Sezione di Bari, Bari, Italy

²⁵ Istituto Nazionale di Fisica Nucleare, Sezione di Firenze, Firenze, Italy

²⁶ Università di Firenze and Istituto Nazionale di Fisica Nucleare, Sezione di Firenze, Firenze, Italy

²⁷ Gran Sasso Science Institute, L'Aquila, Italy and INFN Laboratori Nazionali del Gran Sasso, Assergi, L'Aquila, Italy

²⁸ INFN Laboratori Nazionali del Gran Sasso, L'Aquila, Italy

²⁹ Istituto Nazionale di Fisica Nucleare, Sezione di Lecce, Lecce, Italy

³⁰ Università del Salento and Istituto Nazionale di Fisica Nucleare, Sezione di Lecce, Lecce, Italy

³¹ Istituto Nazionale di Fisica Nucleare, Sezione di Napoli, Napoli, Italy

³² Università di Napoli "Federico II" and Istituto Nazionale di Fisica Nucleare, Sezione di Napoli, Napoli, Italy

³³ Istituto Nazionale di Fisica Nucleare, Sezione di Pavia, Pavia, Italy

³⁴ Istituto Nazionale di Fisica Nucleare, Sezione di Perugia, Perugia, Italy

- 35 Università degli Studi di Perugia and Istituto Nazionale di Fisica Nucleare, Sezione di Perugia, Perugia, Italy
36 Università di Siena and Istituto Nazionale di Fisica Nucleare, Sezione di Pisa, Pisa, Italy
37 Département de Physique Nucléaire et Corpusculaire (DPNC), Université de Genève, Genève, Switzerland
38 Department of Astronomy, University of Geneva, Geneva, Switzerland
39 Centro de Investigaciones Energéticas, Medioambientales y Tecnológicas (CIEMAT), E-28040 Madrid, Spain
40 Dept. Física Quàntica i Astrofísica, Institut de Ciències del Cosmos (ICCUB), Universitat de Barcelona (IEEC-UB), Barcelona, Spain
41 Universitat Pompeu Fabra (UPF), Barcelona, Spain
42 Institut de Física d'Altes Energies (IFAE), The Barcelona Institute of Science and Technology (BIST), E-08193 Bellaterra, Barcelona, Spain
43 KTH Royal Institute of Technology, Stockholm, Sweden
44 Institute of Physics, Ecole Polytechnique Fédérale de Lausanne (EPFL), Lausanne, Switzerland
45 Istituto Nazionale di Fisica Nucleare, Sezione di Trieste, Trieste, Italy
46 Università degli Studi di Napoli Federico II, Napoli, Italy
47 Università degli Studi di Trieste, Italy
48 Italian Space Agency and Istituto Nazionale di Fisica Nucleare, Sezione di Perugia, Perugia, Italy
49 Università degli Studi di Sassari and Istituto Nazionale di Fisica Nucleare, Sezione di Perugia, Perugia, Italy
50 Istituto Nazionale di Fisica Nucleare, Sezione di Roma Tor Vergata, Rome, Italy
51 INFN Sezione di Bologna, 40126 Bologna, Italy
52 INFN Sezione di Bologna, 40126 Bologna, Italy; Università di Bologna, 40126 Bologna, Italy
53 Dipartimento di Fisica e Chimica "E. Segrè" Università degli Studi di Palermo, Palermo, Italy and INFN sez. Catania, Catania, Italy